RSC Advances

ROYAL SOCIETY OF CHEMISTRY

www.rsc.org/advances

Cite this: DOI: 10.1039/c0xx00000x

PAPER

www.rsc.org/xxxxxx

SCO@SiO_2@Au core-shell nanomaterials: enhanced photo-thermal plasmonic effect and spin-crossover properties

Dan Qiu,[a] Ling Gu,[a] Xiao-Li Sun,[a] Dong-Hong Ren,[a] Zhi-Guo Gu,[*a,b] and Zaijun Li[a]

Received (in XXX, XXX) Xth XXXXXXXXX 20XX, Accepted Xth XXXXXXXXX 20XX

DOI: 10.1039/b000000x

We reported here an effective synthetic route to gold coated spin-crossover core-shell nanocomposites (SCO@SiO_2@Au) in which $[Fe(Htrz)_2(trz)](BF_4)$@SiO_2 (SCO@SiO_2) served as a support to Au nanopartilces. The obtained core-shell nanocomposites were studied using numerous characterization techniques to define the structure, morphology, composition and especially the spin-crossover properties. The transmission electron micrographs illustrated that Au nanopartilces with an average diameter around 2.5 nm were decorated uniformly on the surface of SCO@SiO_2. X-ray photoelectron spectroscopy measurements further confirmed the successful incorporation of gold nanoparticles on spin-crossover core. The Raman spectrum indicated that the plasmonic Au nanopartilces made an efficient photo-thermal heating in the SCO@SiO_2@Au nanocomposites, leading to a ~100 times reduction of laser energy needed for spin state switching compared with SCO@SiO_2. The magnetic study demonstrated that the embedded Au nanopartilces not only influenced the spin transition temperatures but also changed the widths of hysteresis loops. SCO@SiO_2@Au nanocomposites may be applied to various areas where the fascinating spin-crossover core and the functional gold shell can be beneficial.

1. Introduction

As frontier of molecular magnetic materials, the spin-crossover complexes (SCO) have received enthusiastic pursuit due to the magnetic bistability and photo-switching capabilities.[1] It is well known that the changes between low spin (LS) and high spin (HS) states in SCO materials can be triggered by external stimuli e.g. temperature change, different degree of pressure, and light irradiation.[2] The triazole-based iron(II) polymeric compounds, as an important member in the SCO system, are still regarded as the ideal materials for technological applications owing to their cooperative spin transition around room temperature with large hysteresis loops and unique color change.[3] A variety of elaborate methods have been applied to manufacture SCO complexes at the nanometer scale for the integration into functional devices.[4] The spin transition temperatures and the widths of the hysteresis loop can be tuned intelligently by the sizes and morphologies of the SCO nanopartilces (NPs).[5] In the numerous merits of triazole-based SCO compounds, the laser-induced spin transition at room temperature is an excellent property for writing and erasing information optically in storage devices.[6] However, the technique is limited to the high laser power needed for inducing the conversion of spin state. Thus, the development of new SCO nanomaterials to diminish the needed laser power for the complete spin state switching is indispensible.

Over the past decades, much significant endeavors have been devoted to the plasmonic NPs which have excellent photo-thermal performance based on the surface plasmons, favoring the different potential applications such as data transport and processing.[7] In the realm of plasmonics, Au NPs have been intensively pursued owing to their facile synthesis, high chemical stability, oxidation resistance, good biocompatibility, useful electronic properties and good affinity.[8] The latter allows Au NPs bind to amine (-NH_2), sulfhydryl (-SH) or carboxyl (-COOH) groups and thus functionalized, making them possible to form hybrid nanomaterials.[9] In particular, the size-dependent surface plasmon resonance (SPR) property of Au NPs exhibiting strong absorbance with tunable wavelength in the near-infrared (NIR) region has been widely studied for photo-thermal therapy.[10] That is, the plasmonic Au NPs as photo-thermal agents induced by the selective laser illumination can control the local heating temperatures in photo-thermal treatment.[11]

On the account of unusual switching characteristics of SCO nanomaterials and parallel to the photo-thermal property of Au NPs, an emerging class of hybrid nanostructure consisting of plasmonic Au and SCO NPs is receiving increasing attention.[12-14] Bousseksou and co-workers have found that the SPR as a powerful tool can be exploited to detect the spin state changes in the SCO NPs with high sensitivity.[12] In the system, molecular spin state switching was efficiently triggered, fast achieved, and highly localized by photo-thermal effect of gold nanorod arrays covered with a thin layer of SCO complex.[13] Recently, the photo-thermal plasmonic effect of Au NPs has also been evidenced on spin state conversion in SCO nanocomposites and the needed laser power intensity reduced 3 times compared with the pure SCO polymers.[14] However, it remains a challenge to develop a more convenient and flexible method to increase the amount of Au NPs on the surface of SCO NPs to modulate their SPR property.

In this contribution, an alternative strategy is proposed to synthesize two different sizes of SCO@SiO2@Au core-shell nanocomposites using an in-situ growth of gold NPs. The Raman signals and spin-crossover behaviors were highlighted significantly to investigate the influence of Au NPs on the spin-crossover properties of nanocomposites. And the efficient spin state switching resulted from the enhanced plasmonic heating effect in SCO/gold nanocomposites will be promising for information storage and other different potential applications.

2. Experimental Section

2.1 Chemical materials

$Fe(BF_4)_2 \cdot 6H_2O$, Htrz (Htrz=1,2,4-triazole), $HAuCl_4 \cdot 4H_2O$, (3-aminopropyl) triethoxysilane (APTES), $NaBH_4$, tetraethyl orthosilicate (TEOS), Triton X-100, n-pentanol, hexamethylene, acetone and ethanol were all reagent grade and purchased from Sigma-Aldrich and used without further purification. Ultrapure milli-Q water (18.2 MΩ. cm) was used in all experiments.

2.2 Apparatus

The fourier transform infrared (FT-IR) were taken from FA-LA2000 FT-IR spectrometer (ABB Bomen Canada) (KBr disk). XRD patterns were collected on a D8 Advance X-ray diffractometer (Bruker AXS Germany) with Cu Kα radiation in a 2θ range from 5° to 90°, and the scan speed was 2° min^{-1}. The size and morphology of the nanocomposites were observed by JEM-2100 (HR) transmission electron microscopy (TEM) (JEOL Japan). The TEM analysis of sample was obtained by dipping a holy grid to NPs ethanol solution and evaporated in air at room temperature. UV-visible absorption spectra were measured in ethanol solution with Shimadzu UV-2101 PC scanning spectrophotometer (Shimadzu Japan). The Raman spectra of the particles deposited on a glass slide were obtained from Invia Raman spectra (Reinshaw England) with 785 nm excitation line. The laser power intensity was adjusted by changing the percentage of 280 mW, the largest laser power intensity in 785 nm excitation line. The laser beam was focused on a ca. 1 μm spot. The data acquisition time used in the measurement was 15 s. Replicate measurements on different areas were made three times to verify that the spectra were a truer presentation of each experiment. Differential scanning calorimeter (DSC) curves were obtained by (PE) DSC-8000 (PE US) from 300 K to 400 K with rate of 10 K min^{-1}. The X-ray photoelectron spectra (XPS) were carried out by Axis Ultra Imaging Photoelectron spectrometer (Kratos Analytical Ltd. Japan), from which can analyze the composition of elements. The magnetic property of nanocomposites was analyzed using a MPMS-XL-7 super strong quantum interference magnetometer (Quantum Design US). The samples were testing at two temperature stages, which were from 300 K to 400 K, and then back to 300 K and the sweep rate is 3 K min^{-1}. The correction of the diamagnetism for the composite material was difficult. Data was corrected for the diamagnetic contribution calculated only from Pascal constants of $[Fe(Htrz)_2(trz)](BF_4)$.

2.3 Synthesis of SCO@SiO_2 NPs

SCO@SiO_2-1: Under nitrogen atmosphere, $Fe(BF_4)_2 \cdot 6H_2O$ (118 mg, 0.35 mmol) resolved in 0.25 mL demineralised water and tetraethyl orthosilicate (TEOS) (0.25 mL) were added dropwise into a mixed solution of Triton X-100 (2 mL), n-amyl alcohol (2 mL), and cyclohexane (8 mL) with stirring to form a clear water-in-oil microemulsion. 0.25 mL aqueous solution of Htrz (73 mg, 1.05 mmol) was added dropwise into the above microemulsion, followed by continuously stirring at room temperature for 24 h in the dark. The color of microemulsion changed from colorless to pink during the reaction suggested that SCO@SiO_2-1 NPs had been fabricated successfully. Finally, the resulting NPs were collected by demulsification (acetone, 5 mL), centrifugation, washed three times with ethanol (8 mL), then redispersed into 4 mL ethanol.

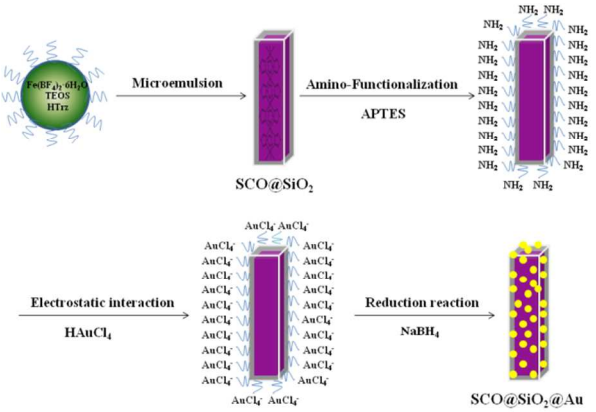

Fig. 1 The synthesis strategy for SCO@SiO_2@Au core-shell nanocomposites.

SCO@SiO_2-2 NPs were prepared by a similar procedure to that described for SCO@SiO_2-1 except the water volume of $Fe(BF_4)_2 \cdot 6H_2O$ and Htrz was changed into 0.2 mL.

2.4 Synthesis of SCO@SiO_2@Au core-shell nanocomposites

SCO@SiO_2@Au-1: The core-shell nanocomposites were prepared by two steps: 1) For the modification with amino groups, 2 mL the previous prepared SCO@SiO_2-1 NPs suspension were redispersed into another 5 mL ethanol by sonication, then 50 μL APTES was added dropwise into the mixture and stirred at room temperature for 12 h. The resulting SCO@SiO_2-NH_2 NPs were washed twice with ethanol (8 mL) and centrifugated, and finally dispersed into 5 mL of ethanol; 2) For the synthesis of gold-coated NPs, 2 mL of 3×10^{-3} M $HAuCl_4 \cdot 4H_2O$ solution prepared at advance and 8 mL demineralised water were added into the above SCO@SiO_2-NH_2 NPs dispersion (1 mL) and stirred at temperature for 0.5 h. Then 0.72 mL of 0.1 M $NaBH_4$ solution was added into the mixed solution and continued reacting 5 min. The solution turned into black once the addition of $NaBH_4$ solution and the change of color indicated the formation of Au NPs. At last, the products SCO@SiO_2@Au-1 were covered by centrifugation, washed three times with ethanol (8mL), and then dried at 60 □ in vacuum overnight.

SCO@SiO_2@Au-2 nanocomposites were prepared by a similar procedure to that described for SCO@SiO_2@Au-1 except SCO@SiO_2-1 was replaced by SCO@SiO_2-2.

3. Results and Discussion

The syntheses procedure of the Au NPs-functionalized SCO@SiO2 core-shell nanocomposites was illustrated in Fig. 1.

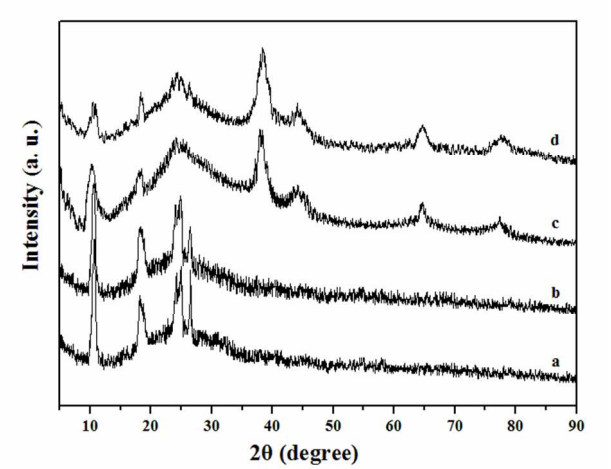

Fig. 2 XRD diffraction patterns of SCO@SiO_2-1 (a), SCO@SiO_2-2 (b), SCO@SiO_2@Au-1 (c), SCO@SiO_2@Au-2 (d).

The fabrication of the SCO@SiO_2 NPs was achieved by a reverse-micelle technique that triazole aqueous solution permeated in the water-in-oil microemulsion droplets including $Fe(BF_4)_2 \cdot 6H_2O$ salt and TEOS.[15] Two subsequent processes of amino-functionalization and electrostatic interaction with $HAuCl_4$ were taken for SCO@SiO_2 NPs core. The silica has been widely used and functionalized as supports for the decoration with gold NPs or gold nanoshell.[16] In our case, the surface modification of SCO@SiO_2 was carried out using APTES as a linker agent, which was known to result in a stable and uniform adsorption of gold NPs.[17] The final gold coated SCO nanocomposites were achieved by reducing the $AuCl_4^-$ anions, and immobilized on the surface of modified cores. In comparison with the published SCO/gold nanocomposites,[14] the synthesis was simplified, and the Au NPs with a small size were formed by in-situ growth and simultaneously anchored to the amino functionalized cores within one step. In addition, the approach promised the attachment of discrete Au NPs onto SCO@SiO2 NPs with forming a full and uniform coating.

FTIR measurements were employed to testify the formation of SCO@SiO_2 NPs and SCO@SiO_2@Au nanocomposites (ESI†) For SCO@SiO_2, two bands observed at ~1453 and ~1496 cm^{-1} corresponded to the ring stretching of 1,2-coordinated triazole ligands, and the peak at ~634 cm^{-1} was the out-of plane vibration of the triazole.[18] While these vibration bands were weakened in the case of SCO@SiO_2@Au nanocomposites. The observed peaks near 1085 cm^{-1} in all samples were anti-symmetric Si-O-Si stretching, indicating the formation of SiO_2.

The powder X-ray diffraction patterns of as-prepared SCO@SiO_2 NPs and SCO@SiO_2@Au nanocomposites were displayed in Fig. 2. For SCO@SiO_2, the obvious diffraction peaks around 2θ at 10°, 18° and 25° corresponded to the positions of the reported $[Fe(Htrz)_2(trz)]BF_4$ micrystalline material.[19] The same peaks were also observed in the SCO@SiO_2@Au nanocomposites. However, compared with SCO@SiO_2, the characteristic peaks were whittled in SCO@SiO_2@Au nanocomposites. This might be explained by the heavy atom effect of Au or the relatively weak intensity between them.[20] After assembling of Au NPs, four characteristic peaks at 38.1°, 44.3°, 64.6° and 77.5° matched the (111), (200), (220) and (311) planes of the gold crystal with a

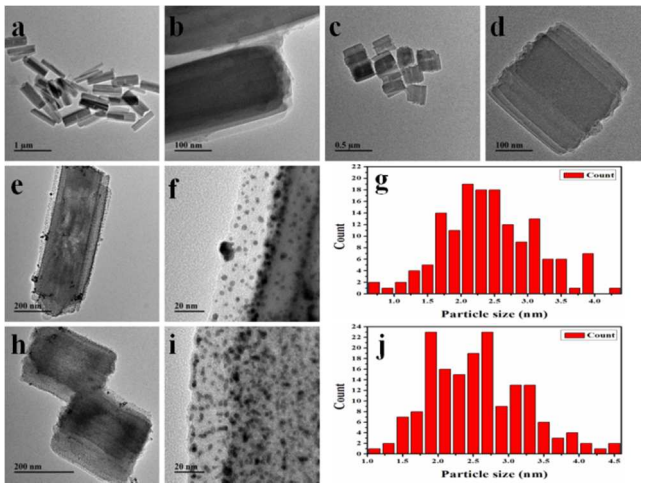

Fig. 3 TEM images of as-prepared SCO@SiO_2-1 (a, b), SCO@SiO_2-2 (c, d), SCO@SiO_2@Au-1 (e, f), SCO@SiO_2@Au-2 (h, i). Size distribution histogram and statistics are for SCO@SiO_2@Au-1 (g) and SCO@SiO_2@Au-2 (j).

cubic phase.[21] In addition, all samples exhibited a very broad peak in the 2θ range from 15° to 30° was assigned to the characteristic diffraction peak of amorphous silica materials. The above analysis indicated that SCO@SiO_2@Au composites were fabricated successfully.

The morphology and structure of the as-synthesized samples were investigated by TEM. The SCO@SiO_2 NPs displayed two different sizes that 750~800 nm length and 150~250 nm width for SCO@SiO_2-1 (Fig. 3a), and 200~250 nm length and 200~230 nm width for SCO@SiO_2-2 (Fig. 3c), which distributed uniformly (Fig. S2). As shown in Fig. 3b and Fig. 3d, SCO@SiO_2-1 NPs exhibited rectangular prisms while SCO@SiO_2-2 NPs appeared as saw-tooth rods. It revealed that not only the sizes but also the shapes of the SCO@SiO_2 NPs were significantly modified by the change of ratio of water to surfactant. TEM images of the SCO nanocomposites showed lots of small and high dispersed Au NPs anchored on the surface of the nanocomposites, owing to their dark image contrast against the support. In particular, as shown in Fig. 3g and 3j, the average diameters of attached Au NPs were ca. 2.44 and 2.55 nm for SCO@SiO_2@Au-1 and SCO@SiO_2@Au-2, respectively. Additionally, it was obvious that the attached Au NPs of SCO@SiO_2@Au-2 were slightly denser than SCO@SiO_2@Au-1 (Fig. 3f and 3i), which might be attributed to the mass ratio of SCO@SiO_2 to $AuCl_4^-$ salt. The different magnification TEM images evidenced the inclusion of the SCO polymers into the silica matrix, from which the narrow outer shell of irregular SiO_2 with ~20 nm thickness were observed surrounding the SCO polymers. The incorporation of silica was also demonstrated in the FT-IR and XRD analysis. Therefore, the analysis of TEM images further revealed that Au NPs were successfully located on the surface of SCO@SiO_2 NPs.

XPS measurements are usually used to analyze the surface characterization of various materials, from which the unambiguous results can be acquired when unique elemental markers present in the various surface components.[16] To further confirm the decoration of Au NPs on the surface of SCO@SiO_2 NPs, the two nanocomposites were given XPS measurements. As shown in Fig. 4a, it was apparent that the based elemental contents in hybrids consisted of C, N, O, Si, Fe and Au. Both of

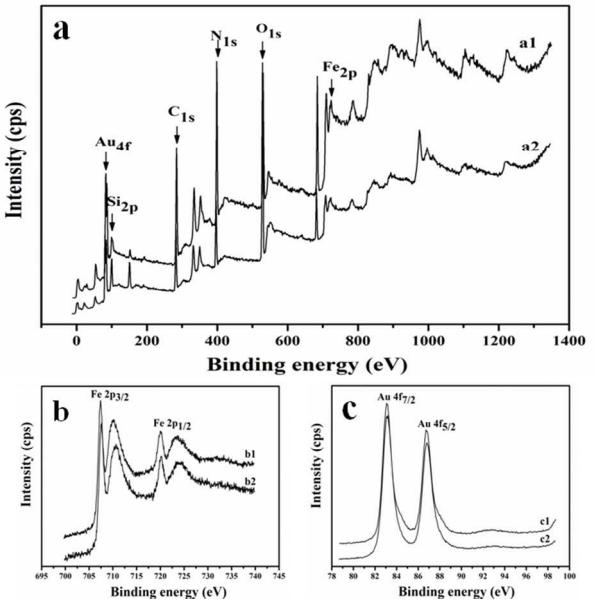

Fig. 4 XPS spectrum of SCO@SiO_2@Au (a) and high resolution spectrum for Fe 2p (b) and Au 4f (c). a1, b1, c1 and a2, b2, c2 correspond to SCO@SiO_2@Au-1 and SCO@SiO_2@Au-2, respectively.

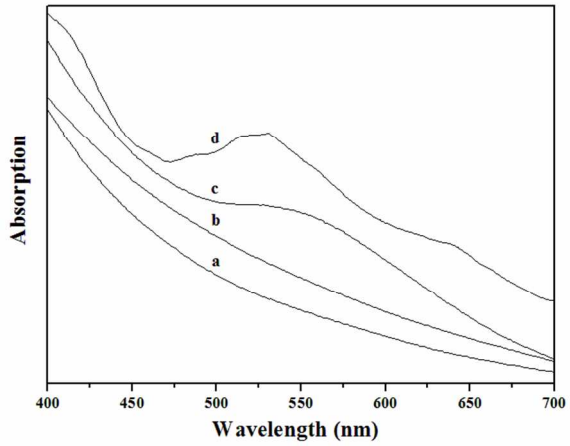

Fig. 5 UV-visible absorption spectra of as-prepared SCO@SiO_2-2 (a), SCO@SiO_2-1 (b), SCO@SiO_2@Au-2 (c) and SCO@SiO_2@Au-1 (d).

SCO@SiO_2@Au-1 (Fig. 4b1) and SCO@SiO_2@Au-2 (Fig. 4b2) showed double peaks at ~707.3 and ~710.3 eV for Fe $2p_{3/2}$, and ~720.0 and 723.5 eV for Fe $2p_{1/2}$. The four binding energy values in the Fe 2p core level spectra were owing to the different spin state of iron spin crossover complexes, that is, ~707.3 and ~720.0 eV for the LS state and ~710.3 and ~723.5 eV for the high HS state.[22] The HS remain at room temperature resulted from the surface partial coordinated Fe atoms, which supported by the high surface area of SCO@SiO_2@Au nanocomposites. In addition, the binding energies at ~83.11 and ~86.81 eV (Fig. 4c) were attributed to the Au $4f_{7/2}$ and Au $4f_{5/2}$,[23] demonstrating that Au NPs were successfully coated on the surface of SCO@SiO_2 NPs. Compared with the metallic Au, the measured binding energies of Au NPs in the two nanocomposites were lower, indicating a negative shift of Au NPs.[24]

Au NPs, as well known, has fascinating optical properties and its optical extinction can be related to the plasmon resonance.[10] The optical properties of nanocomposites with Au NPs coating were

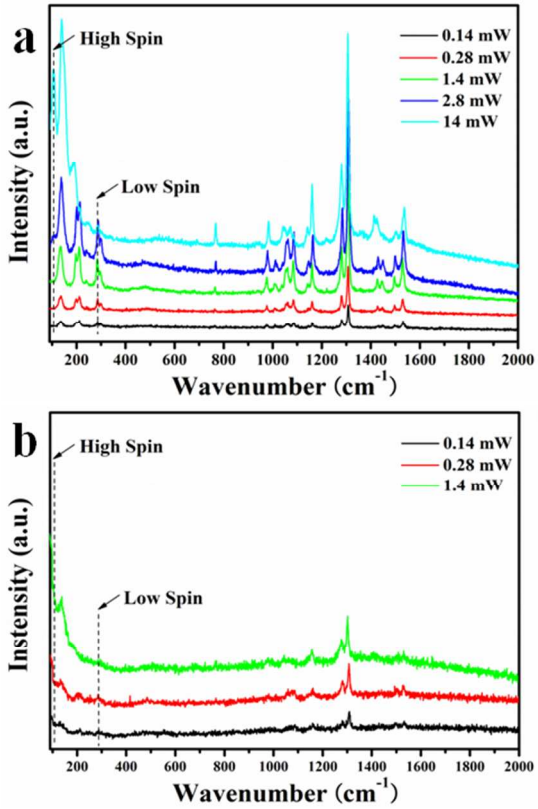

Fig. 6 Raman spectra of as-prepared SCO@SiO_2-1 (a), SCO@SiO_2@Au-1 (b).

carried out via UV-visible absorption spectroscopy. As shown in Fig. 5, SCO@SiO_2@Au-1 exhibited absorption at ~525 nm and the peak was sharp and intense. The absorption peak moved to ~545 nm in SCO@SiO_2@Au-2, which was red-shift and broader attributing to the sensibility of Au NPs. Spherical Au NPs with a diameter of 5 nm presented the surface plasmon band at 520 nm in ethanol while it could be changed by the size, shape, interparticle distance and environment of the particles.[25]

To investigate the laser-induced spin transition and the plasmonic heating effect of Au NPs on SCO@SiO_2 NPs, Raman spectra were obtained by varying the selective output power intensity of Raman laser illumination with 785 nm excitation line. The positions of the samples measured with the various laser power intensities were different to make sure that the testing points were initially in the LS state at room temperature. The most significant characteristics in wavenumber between 100 and 400 cm^{-1} were typically used to indicate the spin transition of iron (II) triazole complexes because of the external metal-ligand vibrational modes.[26] As shown in Fig. 6a and Fig. S3a, for SCO@SiO_2 NPs, the most significant changes observed in the Raman spectra were that the particular vibration modes at 106 cm^{-1} assigned to HS state appeared and 286 cm^{-1} related to the LS state disappeared completely after the laser power intensity approached from 2.8 to 14 mW. This phenomenon demonstrated the achievement of the LS to HS switch. The internal stretching and deformation modes of the triazole ring observed in the spectroscopic region between 900 and 1400 cm^{-1} were no major change in the process of spin conversion of SCO@SiO_2 NPs, except that the bands at 1056 and 1308 cm^{-1} attributed to Htrz and those at 1083 and 1282 cm^{-1} due to trz shifted to the lower

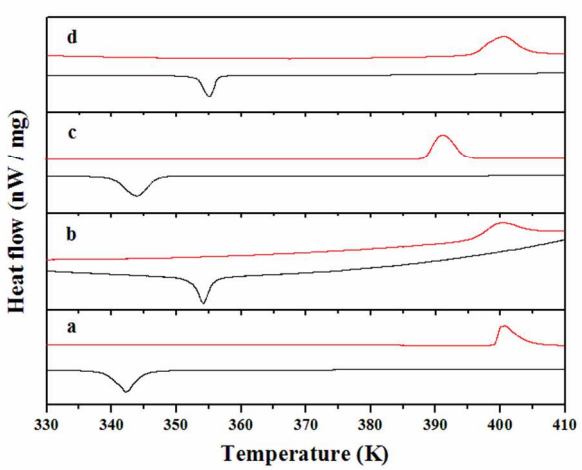

Fig. 7 DSC curves of SCO@SiO_2-1 (a), SCO@SiO_2@Au-1 (b), SCO@SiO_2-2 (c), SCO@SiO_2@Au-2 (d). Red is heating mode, black is cooling mode.

wavenumber lightly (Fig. S3c and Fig. S3e), which also evidenced the spin switching. In the case of SCO@SiO_2@Au nanocomposites, the characteristic Raman bands of [Fe(Htrz)$_2$(trz)](BF_4) complex almost weakened which might be due to the surface-enhanced Raman scattering (SERS) effect (Fig. 6b and Fig. S3b).[27] In other words, the dominant SERS effect associated to the surface contact between the assembling Au NPs and [Fe(Htrz)$_2$(trz)](BF_4) molecules made it difficult to observe the typical Raman signals of [Fe(Htrz)$_2$(trz)](BF_4) polymers. However, it was obvious that SCO@SiO_2@Au nanocomposites displayed strong Raman signal of HS state, which appeared as an upward trend of intensity around at 106 cm^{-1}. And no signal of LS state was observed at 0.14 mW, the lowest laser power intensity to obtain the Raman spectrum. In addition, the Raman signals of Htrz and trz due to HS state in the SCO@SiO_2@Au kept at 1305 and 1278 cm^{-1} (Fig. S3d and Fig. S3f). Therefore, the results demonstrated that a very low laser power could induce the spin state conversion by decorating Au NPs on the surface of SCO@SiO_2 NPs. Compared with SCO@SiO_2 NPs, the decrease of the laser power intensity could be explained by the plasmonic heating effect of Au NPs, which made an efficient photo-thermal heating in the direct vicinity of the SCO@SiO_2@Au nanocomposites, leading to a ~100 times reduction of laser energy needed in spin state switching. Additionally, the needed laser power intensity for SCO@SiO_2@Au nanocomposites reduced substantially in the paper evidenced that the increasing amount of Au NPs could be more effective to control spin switching of SCO polymers according to the reported literature.[14]

DSC curves were performed to check the spin-crossover phase transition temperatures of SCO@SiO_2 NPs and SCO@SiO_2@Au nanocomposites. As shown in Fig. 7, the peaks of phase transition temperatures in the heating and cooling modes of DSC curves were 401 K and 342 K for SCO@SiO_2-1, 391 K and 344 K for SCO@SiO_2-2. Compared with SCO@SiO_2 NPs, it was obvious that the transition temperatures of SCO@SiO_2@Au core-shell nanocomposites shifted slightly to right (Fig. 7b and 7d). The temperatures estimated at 400 K and 401 K in the warming process and 350 K and 355 K in the cooling process for SCO@SiO_2@Au-1 and SCO@SiO_2@Au-2, respectively. The

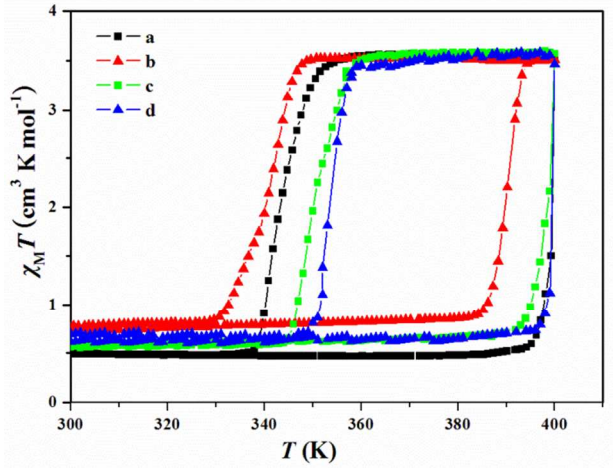

Fig. 8 Plots of $\chi_M T$ versus T for SCO@SiO_2-1 (a, black spheres), SCO@SiO_2-2 (b, red triangles), SCO@SiO_2@Au-1 (c, green spheres), SCO@SiO_2@Au-2 (d, blue triangles).

Table 1 The magnetic data of SCO@SiO_2 and SCO@SiO_2@Au nanoparticles.

	$T_c\uparrow$	$T_c\downarrow$	ΔT
SCO@SiO_2-1	399 K	341 K	58 K
SCO@SiO_2@Au-1	398 K	348 K	50 K
SCO@SiO_2-2	390 K	343 K	47 K
SCO@SiO_2@Au-2	399 K	353 K	46 K

primary DSC results indicated that the presence of Au NPs influenced the magnetic phase transition temperatures of SCO@SiO_2@Au nanocomposites.

To confirm the change of spin-crossover properties by assembling Au on SCO@SiO_2 NPs, the magnetic susceptibilities were measured over the temperature range 300-400K with a heating and cooling sweep. The SCO phenomenon of each sample was clearly displayed by $\chi_M T$ vs T curves (Fig. 8). Different degree remnant of HS residue was observed in the two samples at 300 K, and the higher remnant HS ratios were as expected for SCO@SiO_2-2 with smaller particle size compared with SCO@SiO_2-1, which were demonstrated in the Mössbauer spectra (Fig. S4). The similar phenomenon was shown in SCO@SiO_2@Au, which corresponded to the XPS analysis above. SCO@SiO_2-1 revealed very abrupt and almost complete transition with a large hysteresis loop of ca. 58 K occurring around $T_c\uparrow$ = 399 K in the warming mode and $T_c\downarrow$ = 341 K in the cooling mode. Compared with SCO@SiO_2-1, the two processes of the spin crossover took place with $T_c\uparrow$ = 390 K and $T_c\downarrow$ = 343 K for SCO@SiO_2-2 and its width of the thermal hysteresis was ca. 47 K. The different hysteresis loop width of SCO@SiO_2 might be explained by the different sizes, morphologies, quantity of solvant molecules and the cristallographic defaults of SCO@SiO_2 NPs.[28] With the integration of Au NPs, the transition temperatures of SCO@SiO_2@Au-1 in the heating and cooling cycles were $T_c\uparrow$ = 398 K and $T_c\downarrow$ = 348 K, defining a hysteresis loop of ca. 50 K. While for SCO@SiO_2@Au-2, the spin crossover transition in both of that protocols appeared at $T_c\uparrow$ = 399 K and $T_c\downarrow$ = 353 K with a hysteresis loop width of 46 K. According to the above results, there were significant changes of magnetic properties in the nanocomposites (Table 1). Compared with the pure SCO NPs, the transition temperatures from HS state to LS state in the cooling mode increased 7 K and 10 K for SCO@SiO_2@Au-1 and

SCO@SiO_2@Au-2, respectively. While the temperatures in the warming process of LS state converted into HS state decreased 1 K for SCO@SiO_2@Au-1 and increased 9 K for SCO@SiO_2@Au-2. As a result, the thermal hysteresis width of the hybrids became narrow and shifted to right after coating of Au NPs on SCO@SiO_2. We speculate this change of magnetization in the nanocomposites can be attributed to the increased mass of Au NPs on the surface of SCO@SiO_2 NPs and the good thermal conductivity contribution of Au NPs.

4. Conclusion

In summary, a facile and efficient method was established for the synthesis of SCO@SiO_2@Au core-shell nanocomposites with core spin-crossover and shell SPR properties. The less laser energy consumption of full LS state to HS state transition for SCO@SiO_2@Au nanocomposites verified that the phasmonic heating effect associated to the SPR absorption of Au NPs favored the laser-induced spin transition. The change of hysteresis loops in SCO@SiO_2@Au nanocomposites also confirmed that the surface Au NPs influenced the magnetism behaviors of spin-crossover complexes. The results offered a powerful platform to construct other similar multifunctional spin-crossover nanomarterials, which were looking forward to expanding many potential applications in information storage.

This work was supported by the National Natural Science Foundation of China (21101078 and 21276105), the Program for New Century Excellent Talents in University of China (NCET-11-0657), the Natural Science Foundation of Jiangsu Province (BK2011143), the Fundamental Research Funds for the Central Universities (JUSRP51314B), and the Project for Jiangsu Scientific and Technological Innovation Team.

Notes and references

[a] *School of Chemical and Material Engineering, Jiangnan University, Wuxi 214122, P. R. China. Fax: +86 510 85917763; Tel: +86 510 85917090; E-mail: zhiguogu@jiangnan.edu.cn.*

[b] *The Key Laboratory of Food Colloids and Biotechnology, Ministry of Education, School of Chemical and Material Engineering, Jiangnan University, Wuxi 214122, P. R. China.*

1 (*a*) A. Galet, A. B. Gaspar, M. C. Muñoz, G. V. Bukin, G. Levchenko and J. A. Real, *Adv. Mater.*, 2005, **17**, 2949-2953; (*b*) P. Guionneau, *Dalton Trans.*, 2014, **43**, 382-393; (*c*) J.-F. Létard, *J. Mater. Chem.*, 2006, **16**, 2550-2559.

2 (*a*) P. Gütlich, A. Hauser and H. Spiering, *Angew. Chem., Int. Ed.*, 1994, **33**, 2024-2054; (*b*) M. A. Halcrow, *Chem. Soc. Rev.*, 2011, **40**, 4119-4142; (*c*) *Spin-Crossover Materials: Properties and Application*, ed. M. A. Halcrow, John Wiley & Sons, 2013; (*d*) J. Tao, R. J. Wei, R. B. Huang and L. S. Zheng, *Chem. Soc. Rev.*, 2012, **41**, 703–737. (*e*) J. A. Real, A. B. Gaspar, V. Niel and M. C. Munoz, *Coord. Chem. Rev.*, 2003, **236**, 121-141; (*f*) A. B. Gaspar, V. Ksenofontov, M. Seredyuk and P. Gütlich, *Coord. Chem. Rev.*, 2005, **249**, 2661-2676; (*g*) A. Cannizzo, C. J. Milne, C. Consani, W. Gawelda, C. Bressler, F. van Mourik and M. Chergui, *Coord. Chem. Rev.*, 2010, **254**, 2677-2686; (*h*) O, Sato, J. Tao and Y. Z. Zhang, *Angew. Chem., Int. Ed.*, 2007, **46**, 2152-2187.

3 (*a*) O. Kahn and C. J. Martinez, *Science*, 1998, **279**, 44-48; (*b*) G. Aromi, L. A. Barrios, O. Roubeau and P. Gamez, *Coord. Chem. Rev.*, 2011, **255**, 485; (*c*) O. Roubeau, *Chem.-Eur. J.*, 2012, **18**, 15230; (*d*) L. G. Lavrenova and O. G. Shakirova, *Eur. J. Inorg. Chem.*, 2013, **670**; (*e*) S. Titos-Padilla, J. M. Herrera, X. W. Chen, J. J. Delgado and E. Colacio, *Angew. Chem., Int. Ed.*, 2011, **50**, 3290-3293.

4 (*a*) W. B. Lin, J. W. Rieter, Taylor and M. L. Kathryn, *Angew. Chem., Int. Ed.*, 2009, **48**, 650-658; (*b*) A. Bousseksou, G. Molnár, L. Salmon and W. Nicolazzi, *Chem. Soc. Rev.*, 2011, **40**, 3313; (*c*) M. Cavallini, *Phys. Chem. Chem. Phys.*, 2012, **14**, 11867; (*d*) H. J. Shepherd, G. Molnár, W. Nicolazzi, L Salmon and A. Bousseksou, *Eur. J. Inorg. Chem.*, 2013, 653–661; (*e*) G. Molnár, L. Salmon, W. Nicolazzi, F. Terki and A. Bousseksou, *J. Mater. Chem. C*, 2014, **2**, 1360–1366.

5 (*a*) T. Forestier, S. Mornet, N. Daro, T. Nishihara, S. Mouri, K. Tanaka, O. Fouché, E. Freysz and J.-F. Létard, *Chem. Commun.*, 2008, 4327-4329; (*b*) J. Larionova, L. Salmon, Y. Guari, A. Tokarev, A. Tokarev, K. Molvinger, G. Molnár and A. Bousseksou, *Angew. Chem., Int. Ed.*, 2008, **47**, 8236-8240; (*c*) J. R. Galán-Mascarós, E. Coronado, A. Forment-Aliage, M. Monrabal-Capilla, E. Pinilla-Cienfuegos and M. Ceolin, *Inorg. Chem.*, 2010, **49**, 5706-5714.

6 (*a*) B. Viquerat, J. Degert, M. Tondusson, E. Freysz, C. Mauriac, J.-F. Létard, Appl. Phys. Lett., 2011, **99**, 061908-1/3; (*b*) Y. A. Tobon, C. Etrillard, O. Nguyen, J.-F. Létard, V. Faramarzi, J.-F. Dayen, B. Doudin, D. M. Bassani and F. Guillaume, *Eur. J. Inorg. Chem.*, 2012, 5837-5842.

7 (*a*) S. A. Maier and H. A. Atwater, *J. Appl. Phys.*, 2005, **98**, 011101; (*b*) P. K. Jain, X. Huang, I. H. El-Sayed and M. A. El-Sayed, *Acc. Chem. Res.*, 2008, **41**, 1578-1586; (*c*) R. A. Vaia and J. Baur, *Science*, 2008, **319**, 420; (*d*) E. Ozbay, Science, 2006, 311, 189-193; (*e*) P. K. Jain, X. Huang, I. H. El-Sayed and M. A. El-Sayed, *Plasmonics*, 2007, **2**, 107-118;

8 (*a*) R. Sardar, A. M. Alison, P. Mulvaney and R. W. Murray, *Langmuir*, 2009, **25**, 13840-13851; (*b*) M.-C. Daniel and D. Astruc, *Chem. Rev.*, 2004, **104**, 293-346; (*c*) I. Y. Goon, L. M. H. Lai, M. Lim, P. Munroe, J. J. Gooding and R. Amal, *Chem. Mater.*, 2009, **21**, 673-681.

9 (*a*) Y. Wang, Y. Shen, A. Xie, S. Li, X. Wang and Y. Cai, *J. Phys. Chem. C*, 2010, **114**, 4297-4301; (*b*) R. Klajn, J. F. Stoddart and B. A. Grzybowski, *Chem. Soc. Rev.*, 2010, **39**, 2203-2237.

10 (*a*) L. C. Kennedy, L. R. Bickford, N. A. Lewinski, A. J. Coughlin, Y. Hu, E. S. Day, J. L. West and R. A. Drezek, *Small*, 2011, **7**, 169-183; (*b*) H. Liu, D. Chen, L. Li, T. Liu, L. Tan, X. Wu and F. Tang, *Angew. Chem., Int. Ed.*, 2011, **49**, 891-895; (*c*) H. Ke, J. Wang, Z. Dai, Y. S. Jin, E. Qu, Z. Xing, C. Guo, X. Yue and J. Liu, *Angew. Chem., Int. Ed.*, 2011, **50**, 3017-3021; (*d*) S. Lal, S. E. Clare, N. J. Halas, *Acc. Chem. Res.*, 2008, **41**, 1842-1851.

11 (*a*) J. R. Cole, N. A. Mirin, M. W. Knight, G. P. Goodrich and N. J. Halas, *J. Phys. Chem. C*, 2009, **113**, 12090-12094; (*b*) J. Y. Chen, C. Glaus, R. Laforest, Q. Zhang, M. X. Yang, M. Gidding, M. J. Welch and Y. N. Xia, *Small*, 2010, **6**, 811; (*c*) W. Dong, W. Li, D. Niu, Z. Ma, J. Gu, Y. Chen, W. Zhao, X. Liu, C. Liu and J. Shi, *Adv. Mater.*, 2011, **23**, 5392-5397.

12 G. Félix, K. Abdul-Kader, T. Mahfoud, I. A. Gural'skiy, W. Nicolazzi, L. Salmon, G. Molnár and A. Bousseksou, *J. Am. Chem. Soc.*, 2011, **133**, 15342-15345.

13 K. Abdul-Kader, M. Lopes, C. Bartual-Murgui, O. Kraieva, E. M. Hernández, L. Salmon, W. Nicolazzi, F. Carcenac, C. Thibault, G. Molnár and A. Bousseksou, *Nanoscale*, 2013, **5**, 5288-5293.

14 I. Suleimanov, J. S. Costa, G. Molnár, L. Salmon and A. Bousseksou, *Chem. Commun.*, 2014, DOI: 10.1039/c4cc02652g.

15 D. Qiu, D.-H. Ren, L. G, X.-L. Sun, T.-T. Qu, Z.-G. Gu and Z. L, *RSC Adv.*, 2014, **4**, 31323–31327.

16 (*a*) S. Xuan, Y.-X. J. Wang, J. C. Yu and K. C.-F. Leung, *Langmuir*, 2009, **25**, 11835-11843; (*b*) Y. Wang, Y. Shen, A, Xie, S. Li, X. Wang and Y. Cai, *J. Phys. Chem. C*, 2010, **114**, 4297-4301.

17 T. Sato, D. Brown and B. F. G. Johnson, *Chem. Commun.*, 1997, 1007-1008.

18 P. Durand, S. Pillet, E.-E. Bendeif, C. Carteret, M. Bouazaoui, H. E. Hamzaoui, B. Capoen, L. Salmon, S. Hébert, J. Ghanbaja, L. Aranda and D.Schaniel, *J. Mater. Chem. C*, 2013, **1**, 1933-1942.

19 (*a*) A. Urakawa, W. Van Beek, M. Monrabal-Capilla, J. R. Galan-Mascaros, L. Palin and M. Milanesio, *J. Phys. Chem. C.*, 2011, **115**, 1323-1329; (*b*) A. Grosjean, P. Négrier, P. Bordet, C. Etrillard, D. Mondieig, S. Pechev, E. Lebraud, J.-F. Létard and P. Guionneau, *Eur. J. Inorg. Chem.*, 2013, 796-802.

20 Z. H. Xu， Y. L. Hou and S. H. Sun, *J. Am. Chem. Soc.*, 2007, **129**, 8698.

21 B.-H. Lai, Y.-R. Lin and D.-H. *Chen, Chem. Eng. J.*, 2013, **223**, 418-424.

22 (*a*) L. N. Mazalov, I. P. Asanov and V. A. Varnek, *J. Electron. Spectrosc. Relat. Phenom.*, 1998, **96**, 209-214; (*b*) E. Coronado, M. Giménez-Marqués, C. Martí-Gastaldo, G. M. Espallargas, E. Navarro-Moratalla and J. C. Waerenborgh, *Inorg. Chem.*, 2013, **52**, 8451-8460.

23 (*a*) C.-L. Fang, K. Qian, J. Zhu and S. Wang, *Nanotechnology*, 2008, **19**, 125601; (*b*) J. Zhang, X. Liu, L. Wang, T. Yang, X. Guo, S. Wu, S. Wang and S. Zhang, *J. Phys. Chem. C*, 2011, **115**, 5352-5357.

24 Z. Zhong, J. Ho, J. Teo, S. Shen and A. Gedanken, *Chem. Mater.*, 2007, **19**, 4776.

25 E. Boisselier and D. Astruc, *Chem. Soc. Rev.*, 2009, **38**, 1759-1782.

26 (*a*) T. Forestier, S. Mornet, N. Daro, T. Nishihara, S.-i. Mouri, K. Tanaka, O. Fouché, E. Freysz and J.-F. Létard, *Chem. Commun.*, 2008, **36**, 4327-4329; (*b*) Y. A. Tobon, C. Etrillard, O. Nguyen, J.-F. Létard, V. Faramarzi, J.-F. Dayen, B. Doudin, D. M. Bassani and F. Guillaume, *Eur. J. Inorg. Chem.*, 2012, **35**,5837-5842; (*c*) W. Hellel, A. O. Hamouda, J. Degert, J. F. Létard and E. Freysz, *Appl. Phys. Lett.*, 2013, **102**, 143304; (*d*) A. Urakawa, W. V. Beek, M. Monrabal-Capilla, J. R. Galán-Mascarós, L. Palin and M. Milanesio, *J. Phys. Chem. C*, 2011, **115**, 1323-1329; (*e*) N. O. Moussa, D. Ostrovskii, V. M. Garcia, G. Molnár, K. Tanaka, A. B. Gaspar, J. A. Real and A. Bousseksou, *Chem. Phys. Lett.*, 2009, **477**, 156-159.

27 C. Bartual-Murgui, A. Cerf, C. Thibault, C. Vieu, L. Salmon, G. Molnár and A. Bousseksou, *Microel. Eng.*, 2013, **11**, 365-368.

28 (*a*) J. R. Galán-Mascarós, E. Coronado, A. Forment-Aliaga, M. Monrabal-Capilla, E. Pinilla-Cienfuegos and M. Ceolin, *Inorg. Chem.*, 2010, **49**, 5706-5714; (*b*) F. Volatron, L. Catala, E. Rivière, A. Gloter, O. Stéphan and T. Mallah, *Inorg. Chem.*, 2008, **47**, 6584-6586.

Graphic abstract

SCO@SiO_2@Au core-shell nanomaterials: enhanced photo-thermal plasmonic effect and spin-crossover properties

Dan Qiu, Ling Gu, Xiao-Li Sun, Dong-Hong Ren, Zhi-Guo Gu, and Zaijun Li

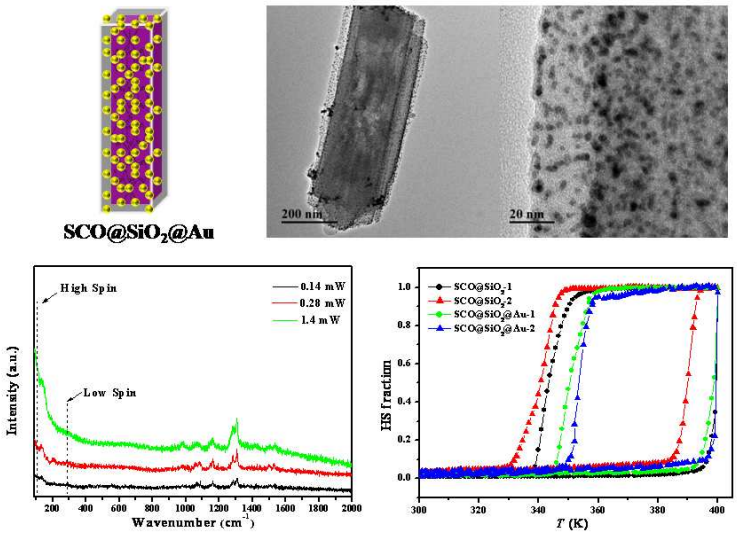

Synopsis

[$Fe(Htrz)_2(trz)](BF_4)$@SiO_2@Au core-shell spin-crossover nanocomposites have been successfully synthesized, and Au nanopartilces made an efficient photo-thermal heating in the nanocomposites and influenced the spin-transition temperatures and the widths of hysteresis loops.